Noise-Driven Oscillations in Coupled Excitable Systems*

Derek Orr[†] and G. Bard Ermentrout[†]

Abstract. In this paper, we investigate a family of coupled excitable cells, using a Kuramoto-type model with either fixed excitability and Gaussian (dynamic) noise or a random distribution of the excitability. In both cases, we reduce the coupled system to a low-dimensional system using mean field approaches such as the Ott-Antonsen ansatz. In the case of a Cauchy distribution of excitability, we prove that with pure sinusoidal coupling, there can be no oscillations. However, if the excitability distribution has faster decay or the noise is Gaussian, then we show that there are oscillations and that they occur in a very specific manner organized around a Takens-Bogdanov bifurcation and a degenerate homoclinic bifurcation. We show that if the coupling is slightly more general, then even a Cauchy distribution is able to generate oscillations. Finally, we rescale the reduced equations in the small heterogeneity limit and show the common dynamics in these different models.

Key words. Ott-Antonsen ansatz, Fokker-Planck, oscillators, mean-field theory, noise, Takens-Bogdanov, bifurcation theory

AMS subject classifications. 34D06, 37G15, 34D20

DOI. 10.1137/20M1358256

1. Introduction. Synchronization of coupled cells can lead to oscillations which are used to transfer and modulate signals throughout most living systems. Noise and heterogeneity are major characteristics of most physical and biological systems; thus, there has been a long time interest in how noise affects oscillatory dynamics ([1, 2, 3, 4]). Many biological systems (such as cardiac cells [5], neurons [6], and other cells [7]) are not intrinsically oscillatory, rather, they are excitable. That is, they have a globally stable rest state and a "threshold." If the threshold is exceeded, there is an amplification of voltage, calcium, or some other quantity, before returning to rest. However, when coupled and driven with noise or heterogeneity, they can often produce synchronized oscillations and other behavior [8, 9, 10, 11, 12, 13, 14]. Sakaguchi [8] was among the first to observe that noise plus coupling can induce oscillations in excitable systems where they performed a bifurcation analysis of a Fourier mode expansion of the associated Fokker-Planck equation. Neiman and collaborators have further analyzed the underlying dynamics of this behavior [9, 11, 15, 16]. Separation of time scales has also been a fruitful approach to this phenomena [12, 14, 17, 18]. In this paper, we will use a mean-field theory (MFT) approach to study the effects of heterogeneity in the excitability as well as Gaussian noise on the emergence of macroscopic oscillations. This approach analyzes the average response over a globally coupled system rather than each individual oscillator

^{*}Received by the editors August 6, 2020; accepted for publication (in revised form) by J. Moehlis January 29, 2021; published electronically May 13, 2021.

https://doi.org/10.1137/20M1358256

Funding: This work was supported by NSF through grant DMS 1951099.

[†]Department of Mathematics, University of Pittsburgh, PA 15620 USA (djo15@pitt.edu, bard@pitt.edu).

and greatly reduces the dimensionality, making it attractive for analysis. MFT has seen a wide variety of applications to the dynamics of large globally coupled biological and physical systems (see [8, 16, 18, 19, 20]). We use the technique developed by Ott and Antonsen [21] which further simplifies the mean-field continuity equations. Their approach has been dubbed the "Ott–Antonsen (OA) ansatz," and it is a very important tool for studying phase oscillations (see [22, 23, 24, 25]).

The excitable cells are all-to-all coupled phase models with a sinusoidal interaction function of the phase differences (Kuramoto model). We start by considering external Gaussian noise, also called dynamic noise, where the noise depends on time (see [20, 26, 27, 28]). We initially apply MFT and simply study the probability density dynamics to find regions in parameter space where there are oscillations. We also investigate other ways to reduce the dimension of this model by truncating it further based on cumulants (see [29]). After this, we employ heterogeneous noise, noise that is independent of time and also labeled "quenched" noise in the physics community, which has been studied in other places in math biology (see [30, 31, 32, 33). We show that the commonly used Cauchy distribution will never give rise to macroscopic oscillations for our coupled excitable system. For other distributions which we describe later, we do find parameters for our system that generate macroscopic oscillations. We remark on the similarities and differences between these distributions as well. Further on, we change the coupling of our model by adding a cosine term, and doing this creates oscillations into the once nonoscillatory Cauchy distribution model. Lastly, in all of the cases that we investigate, the transition to oscillations and their subsequent loss appear to occur via the same mechanism. Thus we perform a rescaling, letting the heterogeneity/noise go to zero, which then simplifies the dynamics and shows the universality of these transitions.

2. Results. We will focus our analysis on the following simple model for a coupled excitable medium:

(2.1)
$$\dot{u}_j = \mu - \cos(u_j) + \frac{c_{ee}}{N} \sum_{k=1}^N H(u_k - u_j) + \eta_j + \xi_j(t), \quad u_j(t) \in S^1 = [0, 2\pi).$$

Here $c_{ee} > 0$ and H(u) is the coupling function which has the form $H(u) = \sin(u) + b(1 - \cos(u))$. The additive term η_j is constant, heterogeneous zero-mean noise, and $\xi_j(t)$ is independent zero mean Gaussian noise with $\langle \xi_j(t)\xi_k(s)\rangle = 2\sigma^2\delta_{jk}\delta(t-s)$. Typically, $0 < \mu < 1$ so that in absence of coupling, there is a stable rest state with $u_j = -\arccos(\mu)$ and an unstable fixed point at $u^+ = \arccos(\mu)$. If initial data are slightly past u^- , then u(t) grows until it reaches $2\pi - u^-$. In the coupled system, noise can cause one or more of the u_j to cross this threshold. The coupling can induce other cells to cross threshold and thus induce a chain reaction that could lead to a synchronous explosion of activity. In the case of heterogeneous noise, for some of the cells, $\mu + \eta_j > 1$, so that in absence of coupling, they will spontaneously oscillate and then the coupling could induce the others to oscillate. There is a balance in the coupling strength, noise, and excitability. If the coupling is too weak, the cells that escape from rest are unable to pull the other cells along, while if it is too strong, the cells will be pinned to the mean state which is at rest. Our goal is to analyze the conditions under which the coupling and noise/heterogeneity balance out enough to generate macroscopic synchronous oscillations in the limit as $N \to \infty$.

2.1. Gaussian noise. We begin with Gaussian noise, $\eta_i = 0$ and use the approach of [8]:

(2.2)
$$\dot{u}_j = \mu - \cos(u_j) + \frac{c_{ee}}{N} \sum_{l=1}^{N} \sin(u_l - u_j) + \xi_j(t),$$

where $\xi_j(t)$ represents time dependent Gaussian noise with mean 0 and variance $2\sigma^2$ as explained above. By taking the limit as $N \to \infty$,

$$\lim_{N \to \infty} \frac{c_{ee}}{N} \sum_{l=1}^{N} \sin(u_l - u_j) = I(t, u) = c_{ee} \int_{-\pi}^{\pi} \sin(v - u) F(t, v) \, dv,$$

where F(t, u) is the probability density for the phase u at time t, and satisfies the nonlinear Fokker-Planck equation (FPE):

(2.3)
$$\frac{\partial}{\partial t}F(t,u) = -\frac{\partial}{\partial u}\left(F(t,u)\left(\mu - \cos(u) + I(t,u)\right)\right) + \sigma^2 \frac{\partial^2}{\partial u^2}F(t,u)$$

as shown in [8, 27, 29]. We further add the conditions that F(t, u) is 2π -periodic in u and is normalized on $[-\pi, \pi]$. Because F(t, u) is periodic, we may assume

$$F(t,u) = \frac{1}{2\pi} \left(\sum_{n=0}^{\infty} a_n(t) \cos(nu) + \sum_{n=1}^{\infty} b_n(t) \sin(nu) \right) = \frac{1}{2\pi} \sum_{n \in \mathbb{Z}} \rho_n(t) e^{-inu}$$

with $\rho_0 = 1$ and $\rho_{-n} = \rho_n^*$. By plugging the Fourier expansion into (2.3) and equating terms, we find

$$\frac{d\rho_n}{dt} = n \left(i\mu \rho_n - \frac{i}{2} (\rho_{n-1} + \rho_{n+1}) - \frac{c_{ee}}{2} (\rho_1^* \rho_{n+1} - \rho_1 \rho_{n-1}) - n\sigma^2 \rho_n \right).$$

Letting $\rho_n = r_n e^{i\theta_n}$, we have equations for the amplitude and phase:

$$\dot{r}_{n} = \frac{n}{2} \left(r_{n+1} \sin(\theta_{n+1} - \theta_{n}) + r_{n-1} \sin(\theta_{n-1} - \theta_{n}) + c_{ee} r_{1} (r_{n-1} \cos(\theta_{n-1} + \theta_{1} - \theta_{n}) - r_{n+1} \cos(\theta_{n+1} - \theta_{1} - \theta_{n})) \right) - n^{2} \sigma^{2} r_{n},
\dot{\theta}_{n} = n\mu - \frac{n}{2r_{n}} \left(r_{n+1} \cos(\theta_{n+1} - \theta_{n}) + r_{n-1} \cos(\theta_{n-1} - \theta_{n}) - c_{ee} r_{1} (r_{n-1} \sin(\theta_{n-1} + \theta_{1} - \theta_{n}) - r_{n+1} \sin(\theta_{n+1} - \theta_{1} - \theta_{n})) \right)$$

with $r_0 = 1$ and $\theta_0 = 0$. By setting $\rho_n = 0$, for all n > 20, we can numerically analyze the resulting truncated system to investigate if oscillations occur when $\mu < 1$. We later remark that we have explored truncations at larger values of n and find no qualitative differences.

Figure 1 summarizes the behavior when σ^2 is fixed (in this case to 0.15) while c_{ee} and μ are varied. The oscillatory behavior is organized around 2 codimension-two bifurcations. First, there is a Takens–Bogdanov (TB) bifurcation (labeled (i)) where the curve of Hopf bifurcations (HBs, in blue) meets with the left-hand fold (red). Emerging from the TB is a curve of homoclinic bifurcations (green curve) that terminates on the right fold (red/purple)

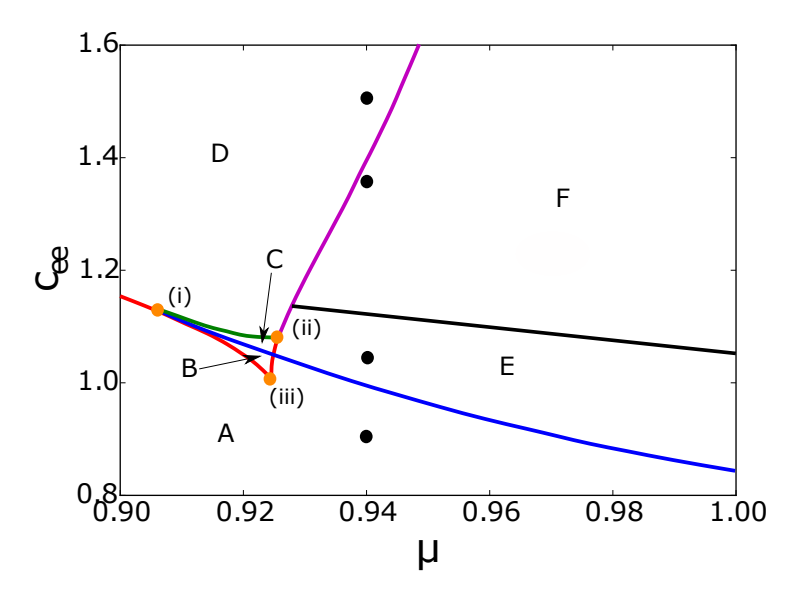


Figure 1. Two-parameter diagram for system (2.4) with $\sigma^2 = 0.15$. In region A, there is a single stable fixed point. As c_{ee} increases into region B, a stable and an unstable fixed point are formed. The blue line is a HB and limit cycles emerge in region C. As c_{ee} continues to increase, the limit cycle undergoes a homoclinic bifurcation. In E, there are also limit cycles; however, opposed to C, these are globally stable. From E to D, there is a SNIC bifurcation and region D contains three fixed points, similar to B. Lastly, region F also contains oscillations; see Figure 3 for more information. The four black dots correspond to the points taken for Figure 4.

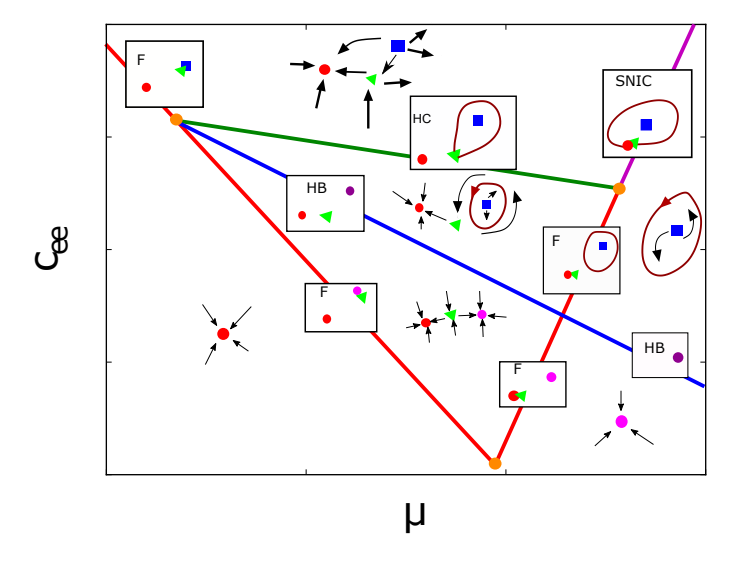


Figure 2. Schematic of the dynamics and transitions of the noisy excitable system overlayed on a zoomed-in simplified version of Figure 1, excluding region F. Filled circles (resp., triangles, squares) are fixed points with no unstable modes (resp., 1, 2). Boxes indicate bifurcations: F, fold; HC, homoclinic; HB, Hopf bifurcation; SNIC, saddle-node infinite cycle.

at point labeled (ii). This is called a noncentral saddle-node homoclinic [34] or a saddle-node loop [35]. We will abbreviate it DH (degenerate homoclinic) for simplicity. In the upper part of the right-hand fold, above the DH there is a transition to periodic orbits via a saddle-node infinite cycle (SNIC) bifurcation and below the DH, oscillations continue from the branch that emanates from the HB. There is a cusp (labeled (iii)), but this plays no role in the oscillations. Oscillations are found in regions C, E, and F. The number of fixed points and their stability is shown in the schematic Figure 2. In region A, there is a single globally stable fixed point; in B, there are two stable fixed points that are separated by a saddle-point; in C, there is bistability between a stable fixed point and a small amplitude limit cycle which arises from an HB from region B. In region D, there is a single stable fixed point and two unstable fixed points. Region E contains macroscopic oscillations and is reached from D via a SNIC bifurcation, from C, via a fold, and from A via a HB. Above region E is region F, where there are still oscillations, although these oscillations are slightly different and pertain to the winding number (see Figure 3). If one were to look at the system in Cartesian coordinates instead of polar coordinates, there would be no bifurcation between region E and region F.

Figure 4 shows the behavior of (2.2) for N=4,000 cells, $\mu=0.94$ and $\sigma^2=0.15$ for different values of c_{ee} . We will denote the Kuramoto order parameter by OP, given as

$$OP = \frac{1}{N} \left| \sum_{j=1}^{N} e^{iu_j} \right|,$$

which is known to be a good measure of synchronization in systems [24]. In Figure 4, we also plot order parameter (OP) for different values of c_{ee} , shown by the dots in Figure 1. Taking $c_{ee} = 0.90$, we are in region A, far from the HB, and the OP shows noisy deviations around a stable fixed point; $c_{ee} = 1.04$ is above the HB curve in region E and shows high frequency noisy oscillations; $c_{ee} = 1.35$ is in region F, and we can see the cells are traversing all angles 0 to 2π , and this point is close to the SNIC curve and shows clear low frequency oscillations; $c_{ee} = 1.5$ is in region D and again shows nearly constant behavior (stable fixed point) where most cells are pinned near a fixed point. The raster plots show the associated behavior of all 4,000 cells for each of these four values of c_{ee} . We note that in the fixed point cases with the lowest and highest coupling are qualitatively different as can be seen in the rasters. In the case of weaker coupling ($c_{ee} = 0.9$), the dynamics are dominated by the noise and each cell fires nearly independently; the result is very asynchronous behavior and a low order parameter (near 0.8). With strong coupling ($c_{ee} = 1.5$), the cells are mainly pinned to the mean phase, $\bar{\theta}$ satisfying $\bar{\theta} = 2\pi - \cos^{-1}(\bar{\mu})$. In this case, the order parameter is high (roughly 0.95) but there are no oscillations; the cells are "synchronized" at the rest state. The OP is nothing more than the amplitude of the first Fourier component of the density, F(t, u) so that oscillations in the OP imply oscillations in the density. As can be seen from the rasters, oscillations in F correspond to synchronous firing of the excitable cells (shown in the rasters as times in which the units pass through π). To better illustrate the dynamics of individual cells in the different regimes, we compute the probability that a cell is at $u = \pi$

$$F(t,\pi) = 1 + 2\sum_{n=1}^{\infty} (-1)^n r_n$$

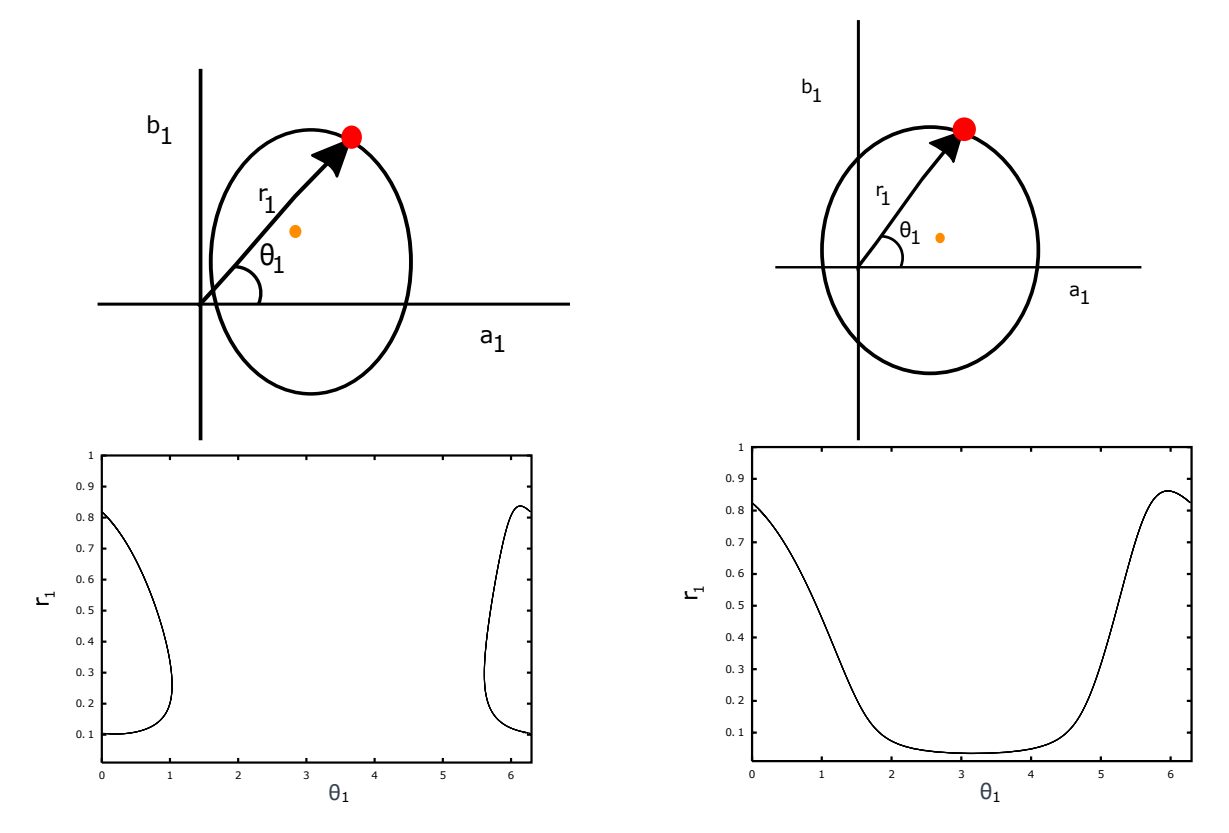


Figure 3. The top left figure is a schematic diagram with parameters in region E, shown in the complex plane. The red dot represents the value of (a_1,b_1) , and this point rotates around the circle as time increases. The black arrow is the vector from the origin to this red point. As the red dot rotates around this limit cycle, the arrow moves as well, changing its magnitude and its direction. The bottom left figure shows the magnitude and direction of the arrow as the red dot rotates around the limit cycle. As c_{ee} increases, we enter region F, whose schematic is shown in the top right picture. Now the limit cycle contains the origin, and because of this, the black arrow rotates around the entire complex plane, as can be seen in the bottom right figure. We can see from the top figures that no bifurcation appears to occur; the limit cycle is simply getting larger as the unstable fixed point (shown in orange) moves. However, from the bottom two figures, one might say that there is a bifurcation occurring between region E and region F. In reality, there is merely a difference in the winding number. Region E has limit cycles with winding number 0 and region E has limit cycles with winding number 1.

and plot it in Figure 5 for the four regimes shown in Figure 4. This allows us to distinguish whether the macroscopic oscillations correspond to synchronous groups of cells firing (going through a complete cycle in phase space) rather than groups of cells making small oscillations around their fixed points. We see from the figure that at low coupling values, $c_{ee} = 0.90$, there is a nonzero probability that any given cell crosses π but these crossings are asynchronous with no macroscopic rhythm. For the two intermediate coupling strengths, $c_{ee} = 1.04, 1.35$, the probability of crossing π varies in time and is periodic with high peaks in F. We note that at the stronger coupling value, the probability of a cell being at π is close to zero for a long stretch of time with brief bouts where the cells fire. This is evident from the raster plots in Figure 4 for $c_{ee} = 1.35$. Finally, at the large coupling strength, $c_{ee} = 1.5$, there are no synchronous firings, and the cells are pinned near rest; the probability of any cell being at

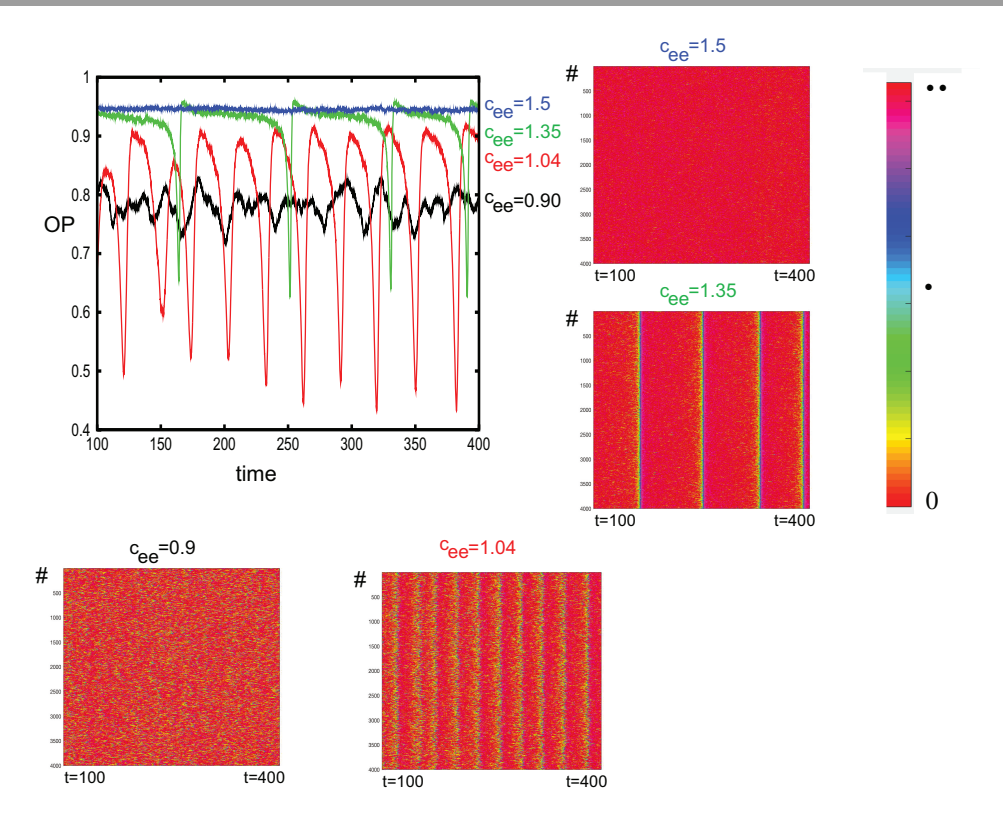


Figure 4. Dynamics of the finite system (N=4,000) of coupled excitable cells ((2.1)) for $\mu=0.94$, $\sigma^2=0.15$, and different values of coupling strength, c_{ee} . The Kuramoto order parameter, $OP=(1/N)|\sum_j \exp(iu_j)|$ is plotted. Raster plot of each of the 4,000 cells are also plotted at the different values of c_{ee} .

 π is very close to zero. In the remainder of the paper, we will use the order parameter as a surrogate for macroscopic oscillations rather than $F(t,\pi)$, mainly because it will turn out to be a key variable in the reduction of the network to a low dimensional system.

Figure 1 remains qualitatively the same as we change the amount of noise. Figure 6 shows a series of two-parameter plots for differing levels of σ^2 . As the noise decreases, the cusp point (intersection of the two red curves) appears to limit to $\mu = 1$ as the noise gets smaller.

2.1.1. FPE truncation. We have approximated the solutions to (2.3) by a finite number of mode equations by setting all modes to zero above n = 20. This is a very simple form of moment closure as one can interpret ρ_n as the expected value of e^{-inu} (the *n*th circular moment). A few natural questions arise: (1) Did we use enough modes? (2) If so, how few are enough to capture the primary dynamics (e.g., the cusp and the TB point)? (3) Are there better ways to truncate the equations?

To answer the first question, we consider a different way to approximate (2.3); we discretize the PDE and compute the bifurcation equations for the resulting system of ODEs. Figure 7A shows a comparison between the 20 mode truncation (used in this section) and the discretization of the PDE, wherein we discretized the PDE into 100 bins. The two plots overlap almost perfectly. This shows that our truncation to 20 modes is not too little at least at the level of noise used in this example ($\sigma^2 = 0.15$).

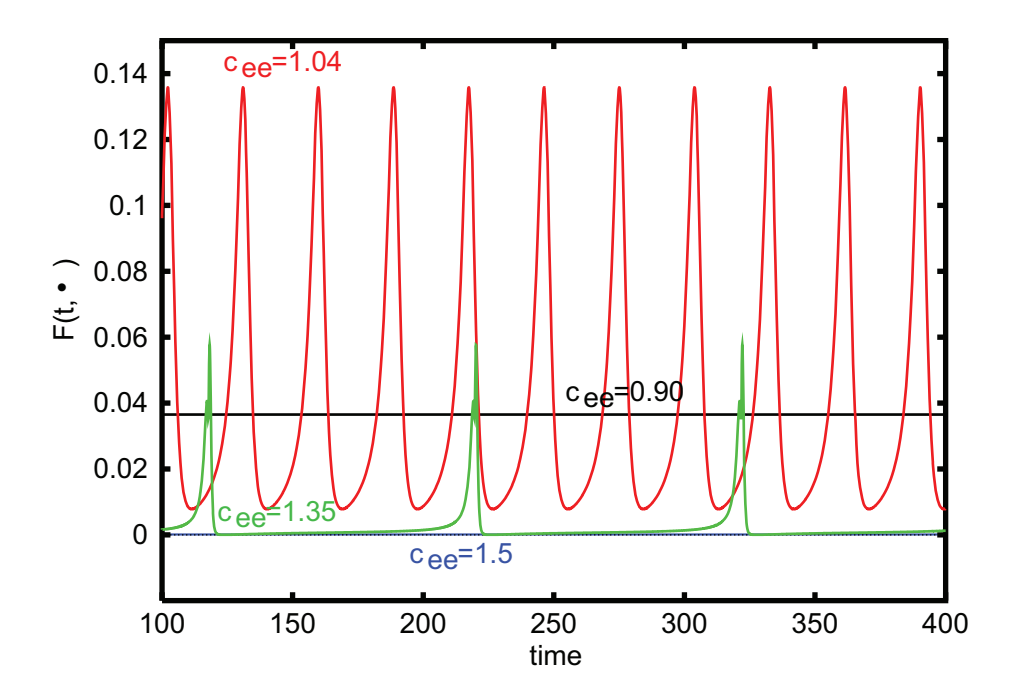


Figure 5. The probability that an oscillator is at $u = \pi$ as a function of time for the same parameters as in Figure 4. One can see qualitatively how the fixed points differ for c_{ee} small and c_{ee} large as well as how $F(t,\pi)$ changes when there are oscillations.

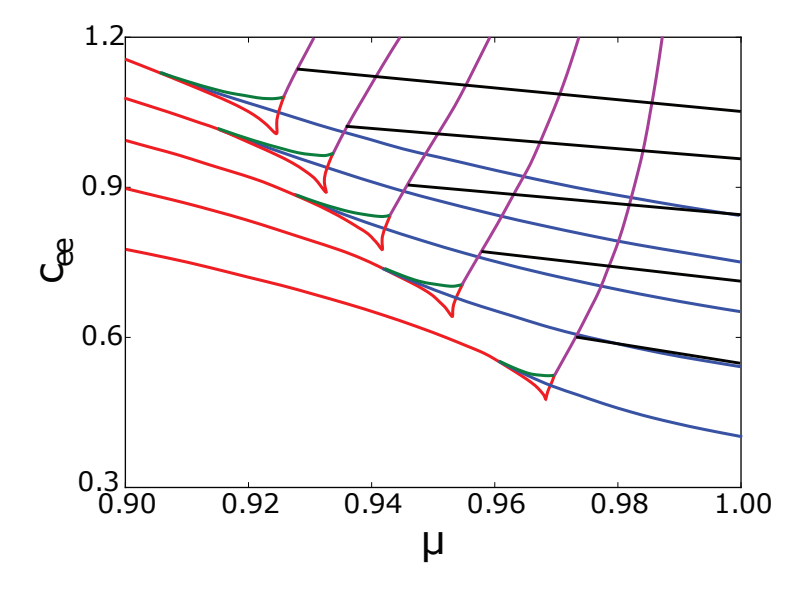
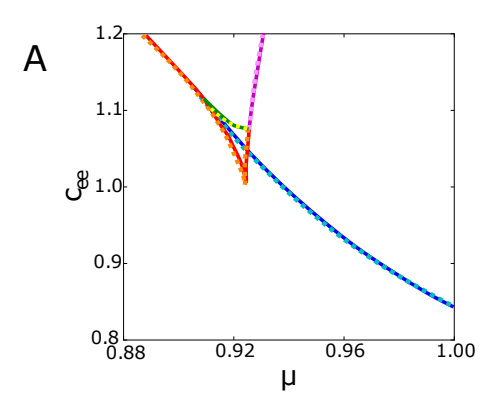


Figure 6. Two-parameter diagram for (2.4) with different noise levels. From top to bottom, the lines touching the c_{ee} -axis correspond to $\sigma^2 = \{0.15, 0.12, 0.09, 0.06, 0.03\}$. As the noise goes to zero, region C shrinks and the cusp tends to $\mu = 1$. We find this to be a common trend for the other systems later in the paper.



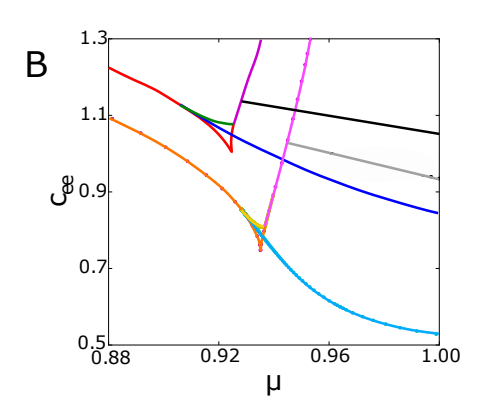


Figure 7. Two parameter diagram for two approximations of (2.3) with $\sigma^2 = 0.15$ (A) Comparison between the 20 mode truncation ((2.4)) and the discretization of the FPE ((2.3)) into 100 bins, which are given square markers and are lighter colored. There is no discernible difference. (B) Comparison of the 20-mode truncation and the 2-mode truncation with cumulant closure.

Let us consider questions 2 and 3. Sakaguchi [8] needed 4 modes to obtain the TB bifurcation using the simple moment closure that $\rho_k = 0$ for k > M. This leads to 8 real ODEs. Suppose that we consider just modes 1 and 2. The equation for ρ_2 involves ρ_3 so we need to express ρ_3 in terms of ρ_1, ρ_2 . The simplest is to just set $\rho_3 = 0$. We have found that this approximation does not work very well and often leads to unbounded behavior, so this is not discussed further. The approximation $\rho_3 = \rho_1^3$ motivated by the so-called OA ansatz (see section 2.2) gives the cusp bifurcation and the TB bifurcation but also has period doubling regimes, other fold bifurcations, other HBs and unbounded areas as well (computations not shown). Recently [29] have suggested that using cumulants rather than moments gives better results. Thus, we suppose that ρ_3 is chosen so that the third order cumulant, $\chi_3 = \rho_3 - 3\rho_2\rho_1 + 2\rho_1^3$, vanishes. That is, we set $\rho_3 = 3\rho_2\rho_1 - 2\rho_1^3$. This simplification results in a system of 4 real ODEs. Figure 7B shows the two-parameter bifurcation structure for the cumulant approximation along with that of the 20-mode truncation for $\sigma^2 = 0.15$. The two plots are qualitatively similar with the same cusp, TB, and homoclinic structures. The differences are seen mostly in the shape of the curves of HB as the noise decreases; they tend to curve quite a bit to the left before terminating at their TB points. Figure 8 goes on to show this and it should be compared to Figure 6; qualitatively the pictures are the same with a TB, cusp, and DH all occurring at each noise level.

In this section, we have shown that there is a particular dynamical structure to systems of coupled excitable cells driven by Gaussian noise. In the next several sections, we show that this is a universal phenomenon and does not depend on the nature of the noise.

2.2. Ott-Antonsen ansatz. We obtained Figure 1 by approximating the solutions to the FPE (2.3) and then analyzing the dynamics of a finite number of Fourier modes. We also looked at a low-dimensional truncation and found qualitatively similar behavior. However, if instead of Gaussian noise, we consider frozen or heterogeneous noise (that is, the noise is taken from some distribution but is constant in time), then it is possible to write down an equation for the Fourier modes which is low dimensional for certain choices of distributions by utilizing the OA ansatz. We now describe this procedure.

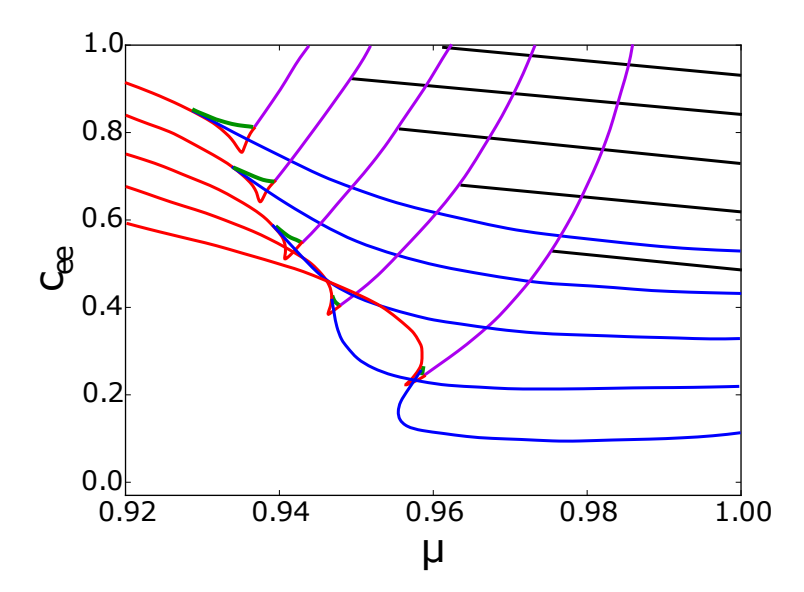


Figure 8. Two parameter diagram for the cumulant closure with different noise levels, $\sigma^2 = \{0.15, 0.12, 0.09, 0.06, 0.03\}$. Compare this to Figure 6. One strange difference is when the noise goes to zero, the HB curve becomes more eccentric and begins at the TB by going back in μ then dipping to a minimum before leaving at $\mu = 1$.

Similarly, we consider a globally coupled population of excitable cells u_j , given by

(2.5)
$$\dot{u}_{j} = \omega_{j} - \cos(u_{j}) + \frac{c_{ee}}{N} \sum_{l=1}^{N} \sin(u_{l} - u_{j}),$$

where ω_j is taken from a distribution with density function $g(\omega)$. Our goal is to study the behavior of these cells as $N \to \infty$. An approach is to use MFT and define the complex order parameter

$$z(t) = \lim_{N \to \infty} \frac{1}{N} \sum_{j=1}^{N} e^{iu_j}.$$

With this, we can look at the asymptotic behavior of z(t) to study the asymptotic behavior of our original system as they will coincide with each other (note that in section 2.1, OP = |z|). Developing a differential equation for z(t) will greatly reduce the dimension of our system as well. As in (2.3), we can write down an equation for the probability density function, $F(u, \omega, t)$, which gives the density at time t of phase u that has fixed frequency ω :

(2.6)
$$\frac{\partial F}{\partial t} + \frac{\partial}{\partial u} (F(u, \omega, t)\dot{u}) = 0,$$

where

$$\dot{u} = \omega - \frac{1}{2}e^{iu} - \frac{1}{2}e^{-iu} + \frac{c_{ee}}{2i}ze^{-iu} - \frac{c_{ee}}{2i}\overline{z}e^{iu}$$

and

(2.7)
$$z(t) = \int_0^{2\pi} \int_{-\infty}^{\infty} F(u, \xi, t) e^{iu} d\xi du.$$

To get the \dot{u} equation, we have used the fact that

$$\lim_{N \to \infty} \frac{1}{N} \sum_{j=1}^{N} \sin(u - u_j) = \int_0^{2\pi} \int_{-\infty}^{\infty} \sin(u - v) F(v, \omega, t) \ d\omega \ dv,$$

written $\sin(u)$ in terms of complex exponentials, and used (2.7). As before, since F is periodic in u and the density of the uncoupled frequencies is known, we write

(2.8)
$$F(u,\omega,t) = \frac{g(\omega)}{2\pi} \left(1 + \sum_{n=1}^{\infty} \alpha_n(\omega,t) e^{-inu} + \overline{\alpha}_n(\omega,t) e^{inu} \right).$$

Because \dot{u} contains only terms in $e^{\pm iu}$, there is an attracting manifold [21] on which $\alpha_n(\omega,t) = \alpha_1(\omega,t)^n \equiv \alpha(\omega,t)^n$. This assumption on the Fourier coefficients is called the OA ansatz, and we will be exploiting it now through most of this paper. One sees immediately that

(2.9)
$$z(t) = \int_{-\infty}^{\infty} \alpha(\omega, t) g(\omega) \ d\omega,$$

so we only need a differential equation for $\alpha(\omega, t)$. Using (2.6) and (2.8) and grouping coefficients of e^{-iu} , we arrive at

(2.10)
$$\frac{\partial \alpha}{\partial t} - i\omega\alpha + \frac{i}{2} + \frac{i}{2}\alpha^2 + \frac{c_{ee}}{2}\alpha^2\overline{z} - \frac{c_{ee}}{2}z = 0.$$

Note that we have reduced the continuity PDE to an infinite set of ODEs for $\alpha(\omega, t)$ that are coupled via the term (2.9). Thus, we still have an infinite number of ODEs to solve. However, if the density $g(\omega)$ has poles in the complex plane, then we can often compute the integral (2.9) using residue theory (this was the crucial observation of [21]). We first consider the Cauchy distribution as that results in the simplest mean-field model, and then we consider several other densities which lead to richer dynamics that are similar to those in section 2.1. Now, suppose

$$g(\omega) := g_0(\omega) = \frac{1}{\pi} \frac{\Delta}{(\omega - \mu)^2 + \Delta^2}$$

with $\Delta > 0$ measuring the spread of g_0 and μ is the center of g_0 . With this, we can evaluate the integral formula for z(t) using contour integrals and the residue theorem. To stay away from the origin, we must integrate around the upper half of the complex plane. Doing this gives $z(t) = \alpha(\mu + i\Delta, t)$, and plugging this into (2.10) gives

(2.11)
$$\dot{z} = (-\Delta + i\mu)z - \frac{i}{2}z^2 - \frac{i}{2}z^2 - \frac{c_{ee}}{2}z^2 \overline{z} + \frac{c_{ee}}{2}z.$$

Let $z(t) = r(t)e^{i\theta(t)}$, and so

(2.12)
$$\dot{r} = -r\Delta - \frac{1 - r^2}{2} \left(\sin(\theta) - c_{ee} r \right),$$

$$\dot{\theta} = \mu - \frac{1 + r^2}{2r} \cos(\theta).$$

Notice if we integrated around the lower half of the complex plane, then the $-r\Delta$ would be replaced by $+r\Delta$ and the magnitude of the order parameter would be larger than 1, which cannot happen by the definition of z(t). Recall that we are interested in whether the combination of noise and coupling is sufficient to drive an excitable network into coherent oscillations. Thus, we are interested in whether or not (2.12) has any kind of periodic behavior for $0 < \mu < 1$, which is the excitable regime. For this planar system there are two ways that oscillations can emerge: (1) HB or (2) drift oscillations via a saddle-node, meaning $\dot{\theta} > 0$ for all time. In what follows, we show that neither of these can occur and more, proving that a Cauchy density cannot produce macroscopic oscillations when the mean μ is in the excitable range.

2.2.1. Analysis of (2.12). We begin by showing there is a positively invariant region.

Lemma 2.1. If $r_0 \in (0,1)$, then $r(t) \in (0,1)$ for all time.

Proof. If $r_0 = 1$, $\dot{r} < 0$ so r(t) decreases. Now let $r_0 = \varepsilon$. Then up to lowest order, we have

$$\begin{split} \dot{r} &= -\frac{1}{2}\sin(\theta) + \mathcal{O}(\varepsilon), \\ \dot{\theta} &= -\frac{1}{2\varepsilon}\cos(\theta) + \mathcal{O}(1). \end{split}$$

If $\theta_0 \in (-\pi/2, \pi/2)$, $\cos(\theta_0) > 0$ and θ will begin to decrease to $-\pi/2$. As θ decreases to $-\pi/2$, $\sin(\theta)$ will become negative and so r will increase. If $\theta_0 \in (\pi/2, 3\pi/2)$, $\cos(\theta_0) < 0$ and θ will increase to $3\pi/2$. As it does, $\sin(\theta)$ will become negative, and r will again increase. So r stays in (0,1).

Now we will prove there are no oscillations for this system. There are three ways for oscillations to exist in this system: One could emerge via a HB, there could be a drift oscillation or there could be some ambient oscillation surrounding a fixed point that never goes away; that is, it exists for any choice of parameters. The outline of the proof will be as follows: We will first prove there are no HBs for any choice of parameters and then show there can be no drift oscillation for $0 < \mu < 1$. The only option is an ambient oscillation. So, for contradiction, we will suppose there is already an oscillation in our system that never vanishes; this oscillation must exist for any parameters we choose. We will show for one set of parameters, there is only one fixed point in $(r, \theta) \in (0, 1) \times (0, 2\pi)$, and it is stable. Thus, no oscillation exists for this set of parameters which would imply no oscillations exist for any set of parameters.

Theorem 2.2. For all c_{ee} , $\Delta > 0$, and $0 < \mu < 1$, there is no HB.

Proof. Letting $\dot{r} = \dot{\theta} = 0$, we have

$$\cos(\theta) = \frac{2\mu r}{1 + r^2}, \qquad \sin(\theta) = c_{ee}r - \frac{2\Delta r}{1 - r^2}.$$

And so.

(2.13)
$$\left(\frac{2\mu r}{1+r^2}\right)^2 + \left(c_{ee}r - \frac{2\Delta r}{1-r^2}\right)^2 = 1$$

must be satisfied. The Jacobian matrix is given by

$$J(r,\theta) = \begin{pmatrix} -\Delta - r(c_{ee}r - \sin(\theta)) + \frac{c_{ee}}{2}(1 - r^2) & -\frac{1}{2}(1 - r^2)\cos(\theta) \\ & \frac{1 - r^2}{2r^2}\cos(\theta) & \frac{1 + r^2}{2r}\sin(\theta) \end{pmatrix},$$

and if we evaluate this at the fixed point,

$$J = \begin{pmatrix} -\Delta - \frac{2\Delta r^2}{1 - r^2} + \frac{c_{ee}}{2}(1 - r^2) & -\frac{\mu r(1 - r^2)}{1 + r^2} \\ \frac{\mu(1 - r^2)}{r(1 + r^2)} & \frac{c_{ee}}{2}(1 + r^2) - \frac{\Delta(1 + r^2)}{1 - r^2} \end{pmatrix}.$$

Define the trace of J as T(r) and the determinant as D(r). We see

$$T(r) = c_{ee} - \frac{2\Delta(1+r^2)}{1-r^2}$$

and

$$D(r) = \left(\frac{c_{ee}}{2}(1-r^2) - \frac{\Delta(1+r^2)}{1-r^2}\right) \left(\frac{c_{ee}}{2}(1+r^2) - \frac{\Delta(1+r^2)}{1-r^2}\right) + \left(\frac{\mu r(1-r^2)}{1+r^2}\right) \left(\frac{\mu(1-r^2)}{r(1+r^2)}\right)$$

$$= \frac{1}{4} \left(T(r) - c_{ee}r^2\right) \left(T(r) + c_{ee}r^2\right) + \frac{\mu^2(1-r^2)^2}{(1+r^2)^2}.$$

We will show that if T(r) = 0; then D(r) < 0. Setting T(r) = 0, the determinant equation and (2.13) become

$$D(r) = -\frac{1}{4}c_{ee}^2r^4 + \frac{\mu^2(1-r^2)^2}{(1+r^2)^2}, \qquad 4\mu^2r^2 + c_{ee}^2r^6 = (1+r^2)^2,$$

respectively. Solving for $c_{ee}^2 r^4/4$ in the second equation and plugging it into the determinant equation, we have

$$\begin{split} D(r) &= -\frac{(1+r^2)^2}{4r^2} + \mu^2 + \frac{\mu^2(1-r^2)^2}{(1+r^2)^2} = \frac{2\mu^2(1+r^4)}{(1+r^2)^2} - \frac{(1+r^2)^2}{4r^2} \\ &= \frac{-8\mu^2r^2(1+r^4) + (1+r^2)^4}{4r^2(1+r^2)^2} = -\left(\frac{8r^2(1+r^4)(1-\mu^2) + (1-r^2)^4}{4r^2(1+r^2)^2}\right) < 0 \end{split}$$

since $0 < \mu < 1$. Thus, there are no Hopf bifurcations.

Theorem 2.3. For all Δ , $c_{ee} > 0$, there are no oscillations provided $0 < \mu < 1$.

Proof. First, notice $\dot{\theta} = 0$ will always have a solution because $\theta = \arccos(\frac{2\mu r}{r^2+1})$ is well-defined since $0 < \mu < 1$. So θ cannot travel around the circle completely without hitting a nullcline. And because there is no HB, the only way for an oscillation to occur is if one has been surrounding a fixed point for all Δ , $c_{ee} > 0$ and $0 < \mu < 1$. In particular, we can choose c_{ee} , Δ , μ , and if there are no oscillations for this particular choice, then there will be no oscillations for any choice. We will begin by showing this system has at least one fixed point.

Motivated by (2.13), define

$$M(r) := \frac{4\mu^2 r^2}{(1+r^2)^2} + r^2 \left(c_{ee} - \frac{2\Delta}{1-r^2}\right)^2 - 1,$$

and notice that the number of solutions to M(r) = 0 for $r \in (0,1)$ corresponds to the number of fixed points in this system. We can see $\lim_{r\to 1^+} M(r) = \infty$ and M(0) = -1. Since it is clear M(r) is continuous on (0,1), by the intermediate value theorem, there will always be at least one fixed point in our system. If we can find a set of parameters where this is the only fixed point in the system and we can prove this fixed point is stable, then we have found one instance where there are no oscillations in our system. Thus, this would prove there are no oscillations for any choice of parameters. We choose $\mu = 0.5$, $c_{ee} = 1$, and $\Delta = 0.5$. Then a fixed point must satisfy $M_0(r) = 0$, where

$$M_0(r) = \frac{r^2}{(1+r^2)^2} + \frac{r^6}{(1-r^2)^2} - 1.$$

Computing the derivative, one finds

$$M_0'(r) = \frac{2r(r^8(1-r^4) + 6r^8 + 4r^6 + 5r^4 + (1-2r^2)^2)}{(1-r^4)^3} > 0$$

since $r \in (0,1)$. Thus, there is only one fixed point. Now we must prove it is stable. For these parameters, the trace and determinant are

$$T_0(r) = 1 - \frac{1+r^2}{1-r^2} = \frac{-2r^2}{1-r^2}$$

and

$$D_0(r) = \frac{1}{4} \left(T_0(r) - r^2 \right) \left(T_0(r) + r^2 \right) + \frac{(1 - r^2)^2}{4(1 + r^2)^2},$$

respectively. Obviously $T_0(r) < 0$ and

$$T_0(r) + r^2 = \frac{-r^2(1+r^2)}{1-r^2} < 0,$$

which means $D_0(r) > 0$; hence this fixed point is stable. So we have found one case where this system has a stable fixed point and so it cannot have oscillations. So, this concludes the entire proof and shows that there are no oscillations in this system for $c_{ee} > 0, \Delta > 0$, and $0 < \mu < 1$.

Summary. In this section we have shown that there are no macroscopic oscillations when (2.5) is in the excitable regime, coupling is purely sinusoidal, and the frequencies follow the Cauchy distribution. From here, there are two ways that we might vary the model equations. First, we could consider a different class of densities, say, with a faster decay than $1/\omega^2$, since it may be that the "fat tails" in the density create too much noise. Another possibility is to change the coupling from $\sin(u)$ to $\sin(u) + b(1 - \cos(u))$ which adds some even terms and does not violate the assumptions needed to make the OA reduction. In the next two sections, we show that either of these assumptions is sufficient to enable macroscopic oscillations when $0 < \mu < 1$.

We add the remark that in the first model (2.4), if we truncated the model even further to $\rho_2 = \rho_1^2$, we arrive at the system (2.12) with $\Delta = \sigma^2$. Because of this, it is more sensible to compare Δ to σ^2 instead of σ when looking at future parameter diagrams in the paper.

2.3. Changing $g(\omega)$. We consider two functionally related densities to that of the Cauchy density, both of which decay like $1/\omega^4$ and thus have thinner tails. In both cases, the dimensionality of the system is doubled, and the analysis is somewhat limited. Nevertheless, we will be able to show that, with these new densities, the behavior is very similar to that of section 2.1. First, consider

$$g(\omega) = g_1(\omega) := \frac{\sqrt{2}}{\pi} \frac{\Delta^3}{(\omega - \mu)^4 + \Delta^4}.$$

Using the residue theorem (see Appendix A), we evaluate (2.9) as

$$z(t) = \frac{1-i}{2}r(t)e^{i\theta(t)} + \frac{1+i}{2}s(t)e^{i\phi(t)},$$

where

$$\dot{r} = -\frac{\sqrt{2}}{2}r\Delta - \frac{1 - r^2}{2}\left(\sin(\theta) - \frac{c_{ee}}{2}r - \frac{c_{ee}}{2}s\cos(\phi - \theta) + \frac{c_{ee}}{2}s\sin(\phi - \theta)\right)$$

$$\dot{\theta} = \mu + \frac{\sqrt{2}}{2}\Delta - \frac{1 + r^2}{2r}\left(\cos(\theta) + \frac{c_{ee}}{2}r - \frac{c_{ee}}{2}s\cos(\phi - \theta) - \frac{c_{ee}}{2}s\sin(\phi - \theta)\right)$$

$$\dot{s} = -\frac{\sqrt{2}}{2}s\Delta - \frac{1 - s^2}{2}\left(\sin(\phi) - \frac{c_{ee}}{2}s - \frac{c_{ee}}{2}r\cos(\theta - \phi) - \frac{c_{ee}}{2}r\sin(\theta - \phi)\right)$$

$$\dot{\phi} = \mu - \frac{\sqrt{2}}{2}\Delta - \frac{1 + s^2}{2s}\left(\cos(\phi) - \frac{c_{ee}}{2}s + \frac{c_{ee}}{2}r\cos(\theta - \phi) - \frac{c_{ee}}{2}r\sin(\theta - \phi)\right).$$

Like the Gaussian case in section 2.1, for a given level of noise and excitability, the coupling strength has to be in a range that is neither too small (cannot overcome noise) or too large (pinned to the rest state).

Figure 9A shows the two-parameter diagram with μ along the x-axis and the coupling, c_{ee} along the y-axis. As with Figure 1, there are 2 codimension-two bifurcations that separate the dynamics. The behavior in each of these regions is the same as the beginning model, shown in Figure 2.

In Figure 9B, we decrease the noise and again, as with Figure 6, the structure of the bifurcation diagram remains. One key feature is as Δ tends to 0, the TB and cusp bifurcation appear to join and form a degenerate codimension-three bifurcation. When we perform

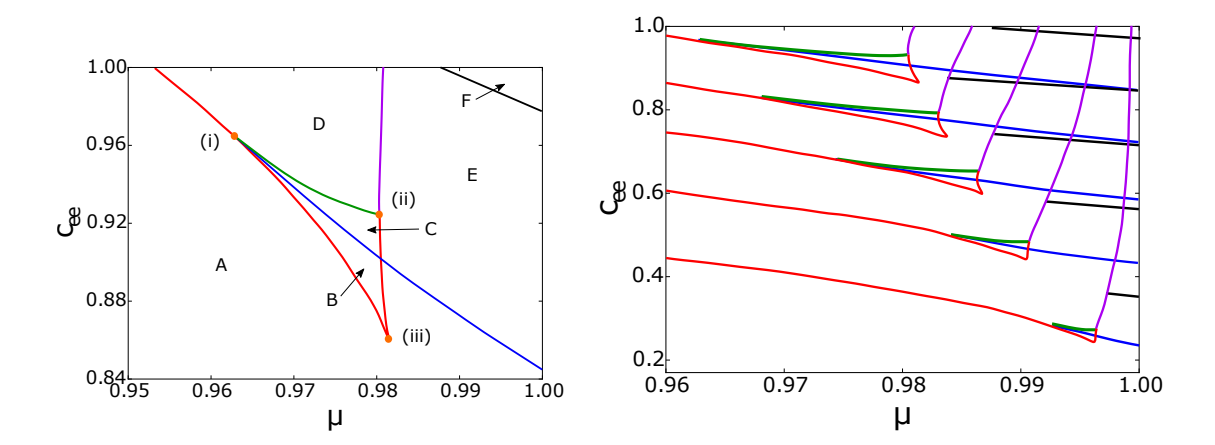


Figure 9. Behavior of (2.14) for different values of excitability, μ , and coupling, c_{ee} when $\Delta=0.27$. Regions and colors as in Figure 1. In the second figure, from top to bottom, the lines that intersect the c_{ee} -axis correspond to $\Delta=\{0.27,0.21,0.15,0.09,0.03\}$. Again, as the noise decreases the region between the homoclinic and Hopf lines also decreases. Further, the cusp bifurcation appears to limit to $\mu=1$ as Δ goes to 0.

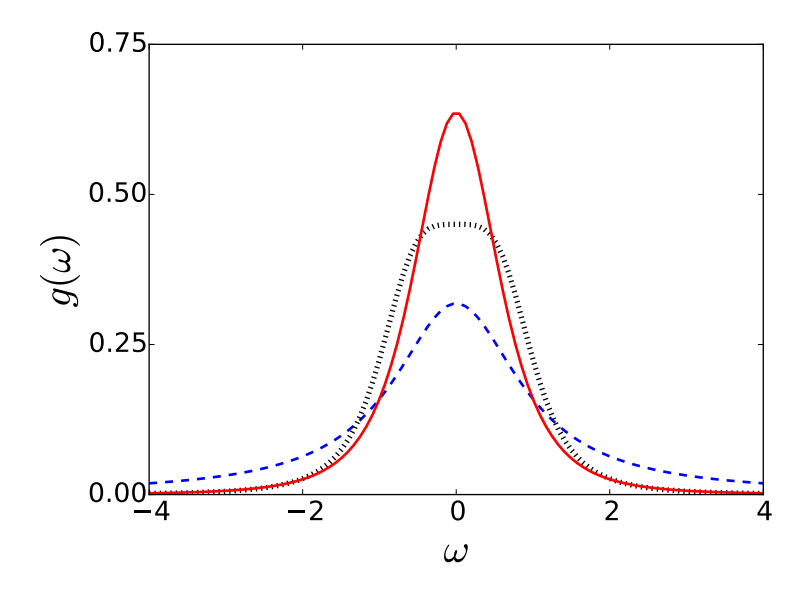


Figure 10. The three densities considered in the paper for heterogeneous noise. In these plots, $\mu = 0$ and $\Delta = 1$. The bottom dashed curve is the original Cauchy density $g_0(\omega)$. The middle dotted graph is $g_1(\omega)$, and the top solid graph is $g_2(\omega)$. As one can see, $g_1(\omega)$ is more flat at 0 but its tails have the same behavior as $g_2(\omega)$.

a rescaling analysis of this system below, we will see that, in fact, the two points remain separated.

Figure 10 shows the densities, $g_0(\omega)$ where there are no oscillations and $g_1(\omega)$ where there are oscillations. The function $g_1(\omega)$ both decays more quickly and has a more uniform density

near $\omega = 0$, thus it is not clear which property of the density allows for synchronization. Thus, we introduce another tractable density (also shown in Figure 10):

$$g(\omega) = g_2(\omega) := \frac{2}{\pi} \frac{\Delta^3}{\left((\omega - \mu)^2 + \Delta^2\right)^2},$$

which has the same decay as $g_1(\omega)$ but also has a more peaked density near $\omega = 0$ like $g_0(\omega)$. As with the other two densities, we can evaluate the integral (2.9) using the residue theorem albeit with a double pole this time. We obtain a modified set of polar equations (see Appendix B for details):

$$\dot{r} = -r\Delta - \frac{1 - r^2}{2} \left(\sin(\theta) - c_{ee}s \cos(\phi - \theta) \right),
\dot{\theta} = \mu - \frac{1 + r^2}{2r} \left(\cos(\theta) - c_{ee}s \sin(\phi - \theta) \right),
\dot{s} = s(r \sin(\theta) - \Delta) + r(\Delta - c_{ee}s^2) \cos(\theta - \phi) - \frac{r^2}{2} \sin(2\theta - \phi)
+ \frac{c_{ee}}{2} s \left(1 + r^2 \cos(2\theta - 2\phi) \right) - \frac{1}{2} \sin(\phi),
\dot{\phi} = \mu + \frac{r}{s} (\Delta - c_{ee}s^2) \sin(\theta - \phi) - r \cos(\theta) + \frac{r^2}{2s} \cos(2\theta - \phi)
+ \frac{c_{ee}}{2} r^2 \sin(2\theta - 2\phi) - \frac{1}{2s} \cos(\phi).$$

We point out that r(t) plays a similar role here as in (2.12); it is magnitude of $\alpha(\omega, t)$ evaluated at the double pole. Once again, we are also able to find oscillatory solutions for $\mu < 1$ that are robust in c_{ee} and Δ . They exhibit very similar dynamics to the previous situation. The key difference is region F begins at lower values of c_{ee} in this scenario. Similar to Figures 6 and 9, as the noise decreases, the cusp bifurcation tends towards $\mu = 1$. The main difference between Figures 9 and 11 is that, although these figures show the same noise, the cusp bifurcation occurs for larger μ in the latter.

We conclude this section with a summary of the coupling induced transitions of (2.14) and (2.15) as this has been the emphasis in several papers such as [11, 12, 14]. Consider a point with μ close to 1 (slightly to the right of the cusps in Figures 9 and 11) and c_{ee} near 0. In this case, there is a single stable fixed point that represents asynchronous behavior (such as seen in Figure 4, $c_{ee} = 0.90$) where r is small and the oscillators behave independently. As c_{ee} increases, we cross the HB and small amplitude macroscopic oscillations emerge. As c_{ee} increases further, the right fold curves are approached and the oscillation frequency decreases but the amplitude increases. Finally, the fold is crossed (a reverse SNIC bifurcation), and there is a single stable fixed point representing the pinned state (c.f. Figure 4, $c_{ee} = 1.5$). Thus, as with the Gaussian noise case, variation in the excitability that decays sufficiently fast leads to the ability of an on average excitable system to generate coherent oscillations when the coupling is neither too weak nor too strong.

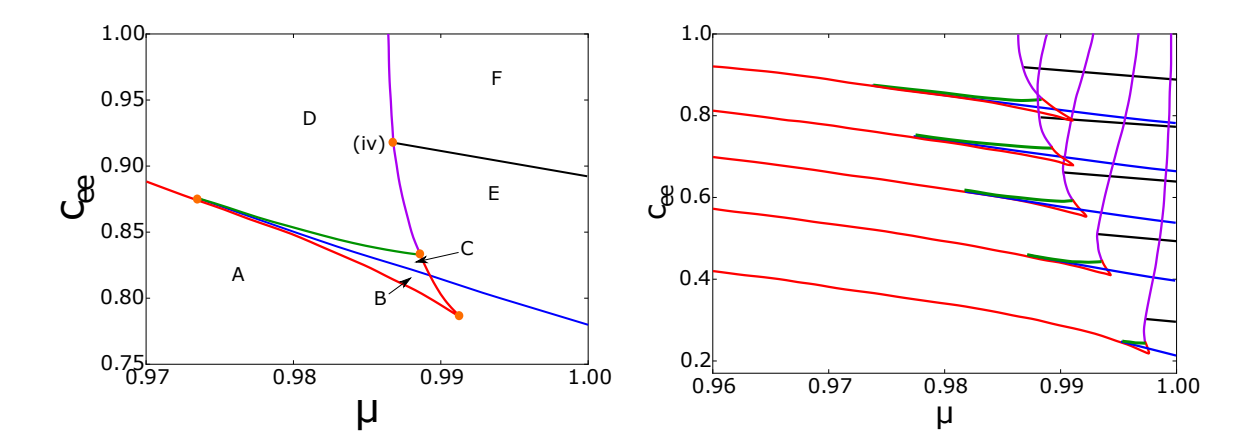


Figure 11. Two-parameter diagram for (2.15) at fixed values of Δ . (Left) $\Delta=0.27$; the lines and regions are exactly comparable to Figures 1 and 9A. One can see the cusp bifurcation occurs for smaller c_{ee} and larger μ than in Figure 9A. (Right) From top to bottom, the lines touching the c_{ee} -axis correspond to $\Delta=\{0.27,0.21,0.15,0.09,0.03\}$, the same noise values as Figure 9B. We also remark that this plot has the same ranges for μ and c_{ee} as in Figure 9B for easy comparison.

2.4. Rescaling analysis. We want to investigate what happens as Δ goes to 0, since it appears the cusp bifurcation and the TB bifurcation meet. We show that this is in fact not the case. One can see that as Δ approaches 0 in each model above, r and s approach 1 and θ and ϕ approach 0. Further, from the previous cascading diagrams, c_{ee} approaches 0 and μ approaches 1. Numerical continuation allows us to guess the proper scaling of the phases, amplitudes, and parameters as $\Delta \to 0$. Thus, we take $\Delta = \varepsilon^2$ and

$$r = 1 + \varepsilon r_1 + \mathcal{O}(\varepsilon^2) \qquad s = 1 + \varepsilon s_1 + \mathcal{O}(\varepsilon^2)$$

$$\theta = \varepsilon \theta_1 + \mathcal{O}(\varepsilon^2) \qquad \phi = \varepsilon \phi_1 + \mathcal{O}(\varepsilon^2)$$

$$c_{ee} = \varepsilon c_1 + \mathcal{O}(\varepsilon^2) \qquad \mu = 1 + \varepsilon \mu_1 + \varepsilon^2 \mu_2 + \mathcal{O}(\varepsilon^3)$$

as the perturbations for our other parameters. In both models, we found $\mu_1 = 0$. Plugging these into (2.14) and grouping orders of ε , we find

(2.16)
$$\dot{r}_{1} = -\frac{\sqrt{2}}{2} - r_{1}(c_{1} - \theta_{1})$$

$$\dot{\theta}_{1} = \mu_{2} + \frac{\sqrt{2}}{2} + \frac{1}{2}\theta_{1}^{2} - \frac{1}{2}c_{1}(r_{1} + \theta_{1} - s_{1} - \phi_{1}) - \frac{1}{2}r_{1}^{2}$$

$$\dot{s}_{1} = -\frac{\sqrt{2}}{2} - s_{1}(c_{1} - \phi_{1})$$

$$\dot{\phi}_{1} = \mu_{2} - \frac{\sqrt{2}}{2} + \frac{1}{2}\phi_{1}^{2} - \frac{1}{2}c_{1}(r_{1} - \theta_{1} - s_{1} + \phi_{1}) - \frac{1}{2}s_{1}^{2}.$$

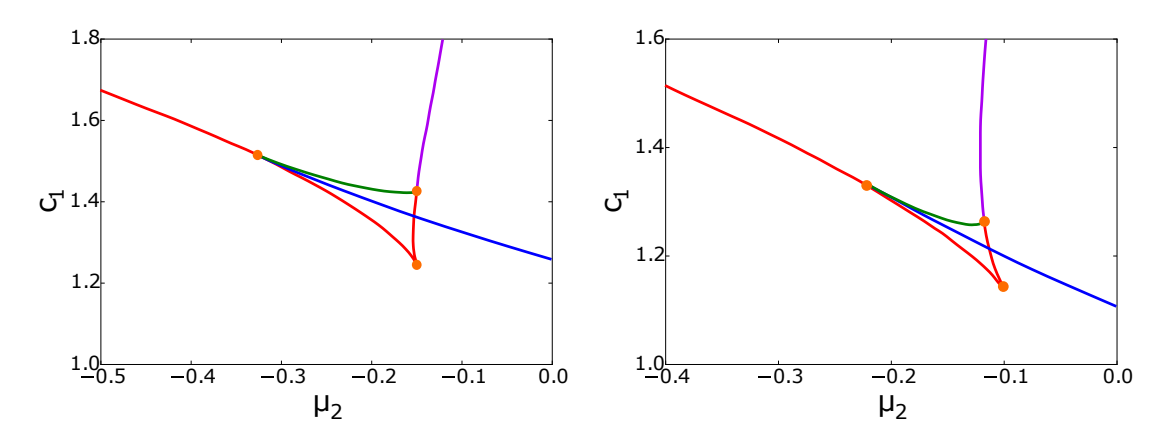


Figure 12. Two-parameter diagram with the rescaled equations, (2.16) on the left and (2.17) on the right. The lines and regions are exactly comparable to Figure 1. One can see $\mu_2 < 0$ which makes sense because μ is approaching 1 from below. In the right-hand system, the equations turn out nicely that one can actually prove the TB point occurs at $(\mu_2, c_1) = (-2/9, 4/3)$ and at the TB, one has $(r_1, \theta_1, s_1, \phi_1) = (-1/2, 5/6, -1, 1/3)$.

Similarly, for (2.15), the rescaled equations are

(2.17)
$$\begin{aligned}
\dot{r_1} &= -r_1(c_1 - \phi_1) - s_1(\phi_1 - \theta_1) \\
\dot{\theta_1} &= \mu_2 - \frac{1}{2}\phi_1^2 + \phi_1\theta_1 - r_1s_1 + \frac{1}{2}s_1^2 \\
\dot{s_1} &= -1 - s_1(c_1 - \phi_1) \\
\dot{\phi_1} &= \mu_2 + \frac{1}{2}\phi_1^2 - c_1(\phi_1 - \theta_1) - \frac{1}{2}s_1^2.
\end{aligned}$$

Figure 12 (left and right) shows the numerical analysis of the rescaled equations, respectively. We can now clearly see that the cusp and the TB points remain well separated as $\Delta \to 0$ and there is no codimension-three bifurcation.

2.5. Changing the coupling. In the previous section, we considered purely sinusoidal coupling between the excitable units; that is, calling $H(\phi)$ the coupling function, we took $H(\phi) = \sin(\phi)$. The coupling function should, in general, satisfy $H(\phi + 2\pi) = H(\phi)$ as the phase space is the circle. Secondly, we assume H(0) = 0 since if H(0) is nonzero, we can incorporate this into the parameter μ . Finally, we want H'(0) > 0 since we want to encourage synchronization. A single odd Fourier mode (e.g., $\sin(\phi)$) can accomplish this. However, in many other studies, the appearance of an even term in the coupling function can have strong qualitative effects on the dynamics ([36, 37, 38]). So, we add a simple even term to the coupling function such that the above constraints hold and further, one for which the OA ansatz can still apply. Hence, we now consider the case where $H(\phi) = \sin \phi + b(1 - \cos \phi)$:

$$\dot{u}_i = \omega_i - \cos(u_i) + \frac{c_{ee}}{N} \sum_{i=1}^{N} \left(\sin(u_j - u_i) + b \left(1 - \cos(u_j - u_i) \right) \right),$$

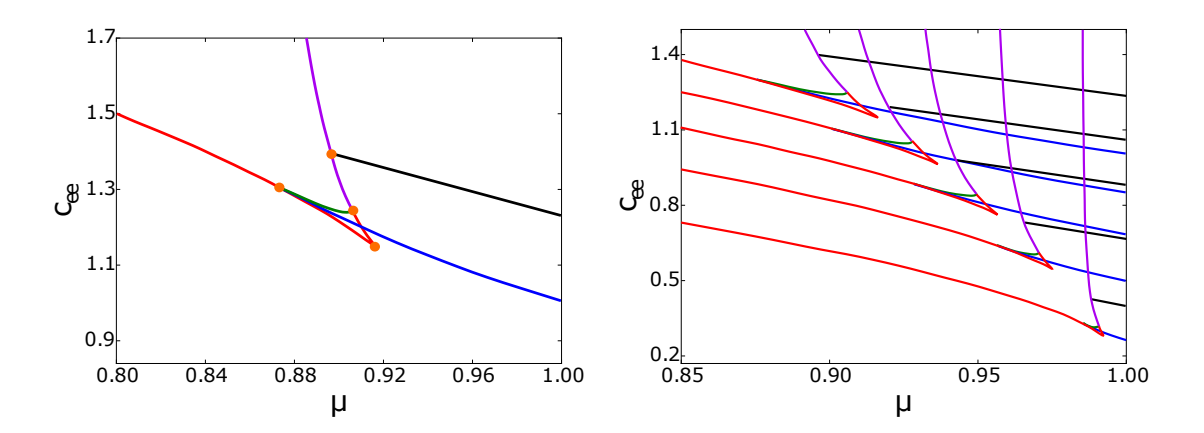


Figure 13. On the left is the bifurcation diagram for system (2.18) with b=0.5 and $\Delta=0.27$. We see the same regions as in Figure 9A. On the right is the cascade diagram for system (2.18) with b=0.5. From top to bottom, the lines touching the c_{ee} -axis correspond to $\Delta=\{0.27,0.21,0.15,0.09,0.03\}$, just as the other figures. Again, as the noise decreases, the homoclinic and HB line get closer to each other. One difference is for fixed Δ , c_{ee} is larger and μ is smaller than the previous cascades.

where b is an extra parameter. We remark that this is equivalent to taking $H(\phi) = \sin(\phi + \gamma) - \sin(\gamma)$. Letting $N \to \infty$ and applying the OA reduction, we arrive at

(2.18)
$$\dot{r} = -r\Delta - \frac{1 - r^2}{2} \left(\sin(\theta) - c_{ee} r \right) \\ \dot{\theta} = \mu + \frac{c_{ee}b}{2} (1 - r^2) - \frac{1 + r^2}{2r} \cos(\theta).$$

For b > 0, there are oscillations in this system as can be seen in Figure 13 where we have set b = 0.5. The two parameter diagram is essentially identical to the ones that we have previously encountered with oscillations between the blue and green curves and to the right of the purple curve and above the blue curve.

As in the previous cases, we can do a rescaling analysis in the limit as $\Delta \to 0$ for nonzero b to see if the TB point and cusp point meet. Again, we have $\Delta = \varepsilon^2$ and

$$r = 1 + \varepsilon r_1 + \mathcal{O}(\varepsilon^2) \qquad \theta = \varepsilon \theta_1 + \mathcal{O}(\varepsilon^2)$$

$$c_{ee} = \varepsilon c_1 + \mathcal{O}(\varepsilon^2) \qquad \mu = 1 + \varepsilon^2 \mu_2 + \mathcal{O}(\varepsilon^3)$$

and the rescaled equations become

(2.19)
$$\dot{r_1} = -1 - r_1(c_1 - \theta_1) \dot{\theta_1} = \mu_2 + \frac{1}{2}\theta_1^2 - bc_1r_1 - \frac{1}{2}r_1^2.$$

We now a have a simple planar quadratic system whose behavior is much easier to analyze than (2.18). Indeed, we can find both the TB, (μ_{TB}, c_{TB}) and the cusp, (μ_{cusp}, c_{cusp}) point for

this system. For notational simplicity, we drop the subscripts in (2.19). The Jacobian matrix at an equilibrium is

$$J(r,\theta) = \begin{pmatrix} \theta - c & r \\ -r - bc & \theta \end{pmatrix}.$$

For an HB, it is necessary that the trace vanish and the determinant be positive. The trace vanishes when $\theta = c/2$ which implies r = -2/c from $\dot{r} = 0$. Setting $\dot{\theta} = 0$ and solving for μ we have

$$\mu_H = \frac{16 - c^4 - 16bc^2}{8c^2}.$$

Furthermore, the determinant,

$$D_H = \frac{16 - c^4 - 8bc^2}{4c^2}$$

must be positive. Since, we want to be in the excitable range where, $\mu_H < 0$, we require that b > 0. One would have to compute the normal form coefficients to determine if this was a generic HB; we will not do that calculation. Numerically, the bifurcation appears to be supercritical. To find the TB point, we set $D_H = 0$ and thus obtain

$$\mu_{TB}(b) = -b,$$
 $c_{TB}(b) = 2\sqrt{-b + \sqrt{b^2 + 1}}$

or

$$c_{TB}(\mu) = 2\sqrt{\mu + \sqrt{\mu^2 + 1}}.$$

Since $\mu_{TB}(b) = -b$, the TB point occurs in the excitable range when b > 0 and so there will always be oscillations for b > 0. Unfortunately, we were not able to find the fold and HBs for fixed b; however, with some algebra, we can find the curve of cusp bifurcations given below:

$$c_{cusp}(\mu) = \sqrt{2\left(D + \sqrt{\frac{(2\mu - D)((D + \mu)^2 + 9)}{D}}\right)},$$

where

$$D = D(\mu) = \operatorname{sgn}(\mu)\sqrt{\mu^2 - 3 + 3(1 + \mu^2)^{2/3}}.$$

The proof of this cusp curve as well as some algebraic facts are given in Appendix C. Notice c_{cusp} is in terms of μ ; we weren't able to solve for μ_{cusp} and c_{cusp} in terms of b specifically. The cusp curve and the curve of TB bifurcations are plotted in Figure 14 as the stippled curves that follow the numerically computed values. As a final remark, we note that we derived equations similar to (2.14) and (2.15) for the case where the coupling has the additional even terms. We have found no qualitative differences from the b=0 case and suspect oscillation regimes remain robust for any $b \in \mathbb{R}$, even for b large and negative. In conclusion, we have shown that by either changing the form of the coupling or the decay of the heterogeneity, we are able to obtain oscillatory behavior in globally coupled excitable cells when the coupling and noise lie within a certain range.

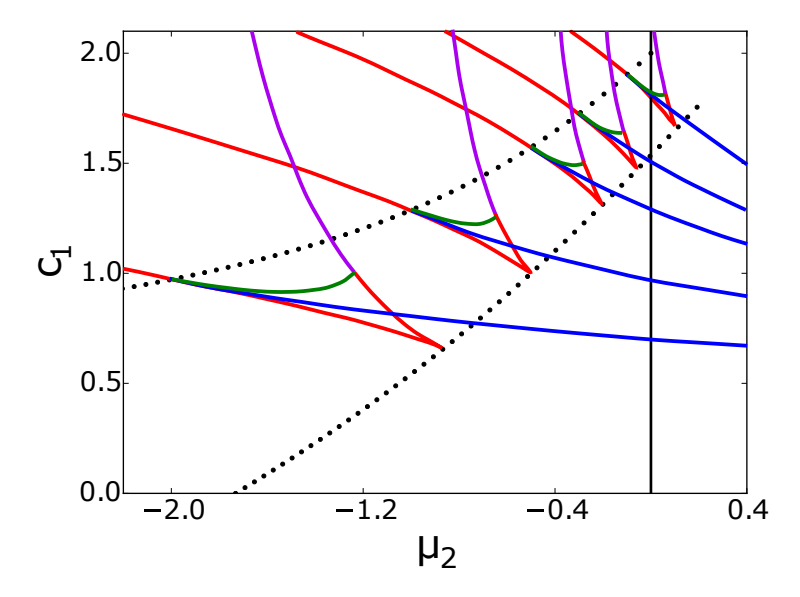


Figure 14. The figure shows the bifurcation diagram for different values of b for the rescaled equations (2.19). From top to bottom, the clusters of graphs correspond to $b = \{0.1, 0.3, 0.5, 1.0, 2.0\}$. As long as the TB point is on the left side of the c_1 -axis, there will be oscillations in the original system. Analytically one can calculate and show that $\mu_{TB}(b) = -b$, meaning there are always oscillations as long as b > 0. We also have plotted the curve of TB curves and cusp curves for $b \ge 0$. When b = 0, the TB curve begins at $(\mu_2, c_1) = (0, 2)$ and the cusp curve begins at $(\mu_2, c_1) = (3^{-3/2}, 4(3^{-3/4}))$. As b increases, the TB and cusp points move to the left and down, with the TB point continuing off to $(-\infty, 0)$ and the cusp point getting infinitesimally close to $(-\sqrt{3}, 0)$.

3. Conclusion/Discussion. In this paper, we described a number of paths to synchronous oscillations in a globally coupled network of excitable elements that were driven either by Gaussian noise or by heterogeneity of parameters. There were essentially three parameters of interest: the mean degree of excitability μ , the coupling strength c_{ee} , and the strength of the noise Δ or σ^2 . When the average cell was in the excitable regime, then noise is required to drive it to fire and coupling is necessary to drive others to fire. If the noise and coupling are in the correct regime, then macroscopic oscillations emerged as seen in Figure 4. In order to better understand this phenomenon, we let the number of cells grow to infinity and described a series of mean-field models. For Gaussian noise, we derived a FPE and from this arose a finite set of equations for the Fourier modes. We showed that macroscopic oscillations existed and were organized around 2 codimension-two bifurcations: the TB and the noncentral saddlenode homoclinic (DH). We also considered a highly reduced version of this that considered only the first two Fourier modes and used a recently devised moment-closure assumption. This system also had the same dynamics and transitions as the coupling and excitability varied. We remark that this moment-closure result [29] could also have heterogeneous noise and this could be explored more but we don't expect the qualitative behavior to change.

In the case of heterogeneous noise, where parameters are taken from a distribution, there is an exact mean-field reduction, and we explored the behavior, first of the Cauchy distribution (section 2.2) and then of some different distributions whose tails decayed faster. In the former case, we obtained a planar dynamical system and showed that there are no macroscopic oscillations possible. However, in the other two distributions, we again had essentially the same dynamics as in the Gaussian noise case with the results that there were synchronized oscillations. With the Cauchy distribution, we used a more general coupling function that was still amenable to the OA reduction and from this, we were able to recover the same bifurcation structure as in the other models. Finally, in the case of the heterogeneous noise models, we were able to perform a rescaling analysis in the limit of narrow spread of heterogeneity, and this analysis again showed the underlying organizing dynamics.

There are several ways one could extend the present work. Here we have considered a single population of cells that are on average excitable. Many biological systems contain mixtures of cells that are spontaneously active (pacemakers) so one could use similar methods to consider systems with, say, two populations of cells whose means are such that they are oscillatory on average. We could then look at various types of interactions such as n:m-locking between the oscillatory and excitable populations [39]. In the simplest such scenario, we could just periodically force all the cells in (2.1) and explore how the heterogeneity in the excitable cells disrupts the different locking regimes. Another more ambitious extension of the present work is to assume that the network is not globally connected but rather distributed in space. Coombes and Byrne [40] as well as others [41] have described methods for extending the OA approach to spatially distributed networks. Then, we might expect to see the spontaneous generation of waves in addition to synchrony.

Appendix A. Residue theory for $g_1(\omega)$. To arrive at (2.14), we use the residue theorem and take the contour around the upper half of the complex plane to get

$$\begin{split} z(t) &= \int_{-\infty}^{\infty} \alpha(\omega,t) g(\omega) \; d\omega = 2\pi i \frac{\Delta^3 \sqrt{2}}{\pi} \bigg(\lim_{\omega \to \mu + e^{i\pi/4} \Delta} \frac{(\omega - \mu - e^{i\pi/4} \Delta) \alpha(\omega,t)}{(\omega - \mu)^4 + \Delta^4} \\ &\quad + \lim_{\omega \to \mu - e^{-i\pi/4} \Delta} \frac{(\omega - \mu + e^{-i\pi/4} \Delta) \alpha(\omega,t)}{(\omega - \mu)^4 + \Delta^4} \bigg) \\ &= 2\pi i \frac{\Delta^3 \sqrt{2}}{\pi} \bigg(\alpha \left(\mu + e^{i\pi/4} \Delta, t \right) \lim_{\omega \to \mu + e^{i\pi/4} \Delta} \frac{1}{4(\omega - \mu)^3} \\ &\quad + \alpha \left(\mu - e^{-i\pi/4} \Delta, t \right) \lim_{\omega \to \mu - e^{-i\pi/4} \Delta} \frac{1}{4(\omega - \mu)^3} \bigg) \\ &= i \frac{\sqrt{2}}{2} \bigg(e^{-3i\pi/4} \alpha \left(\mu + e^{i\pi/4} \Delta, t \right) - e^{3i\pi/4} \alpha \left(\mu - e^{-i\pi/4} \Delta, t \right) \bigg). \end{split}$$

And so we find $z(t) = \gamma z_1 + \overline{\gamma} z_2$ where $z_1 = \alpha(\mu + e^{i\pi/4}\Delta, t)$, $z_2 = \alpha(\mu - e^{-i\pi/4}\Delta, t)$ and $\gamma = i\sqrt{2}/2e^{-3i\pi/4} = 1 - i/2$. Plugging these into (2.10), we see

(A.1)
$$\dot{z}_{1} = i\left(\mu + e^{i\pi/4}\Delta\right)z_{1} - \frac{i}{2}z_{1}^{2} - \frac{c_{ee}}{2}z_{1}^{2}(\overline{\gamma z_{1}} + \gamma \overline{z_{2}}) - \frac{i}{2} + \frac{c_{ee}}{2}(\gamma z_{1} + \overline{\gamma} z_{2})$$
$$\dot{z}_{2} = i\left(\mu - e^{-i\pi/4}\Delta\right)z_{2} - \frac{i}{2}z_{2}^{2} - \frac{c_{ee}}{2}z_{2}^{2}(\overline{\gamma z_{1}} + \gamma \overline{z_{2}}) - \frac{i}{2} + \frac{c_{ee}}{2}(\gamma z_{1} + \overline{\gamma} z_{2}).$$

Writing $z_1(t) = r(t)e^{i\theta(t)}$ and $z_2(t) = s(t)e^{i\phi(t)}$, we separate real and complex parts and arrive at (2.14).

Appendix B. Residue theory for $g_2(\omega)$. The main difference in deriving (2.15) is that there is a pole of order 2 instead of order 1. Again taking the contour around the upper half of the complex plane, we see

$$z(t) = \int_{-\infty}^{\infty} \alpha(\omega, t) g(\omega) \ d\omega = 2\pi i \frac{2\Delta^{3}}{\pi} \left(\lim_{\omega \to \mu + i\Delta} \frac{\partial}{\partial \omega} \left[\frac{(\omega - \mu - i\Delta)^{2} \alpha(\omega, t)}{\left((\omega - \mu)^{2} + \Delta^{2}\right)^{2}} \right] \right)$$

$$= 4\Delta^{3} i \lim_{\omega \to \mu + i\Delta} \frac{\partial}{\partial \omega} \left[\frac{\alpha(\omega, t)}{(\omega - \mu + i\Delta)^{2}} \right] = \lim_{\omega \to \mu + i\Delta} \left(\frac{4\Delta^{3} i}{(\omega - \mu + i\Delta)^{2}} \frac{\partial \alpha}{\partial \omega} (\omega, t) - \frac{8\Delta^{3} i \alpha(\omega, t)}{(\omega - \mu + i\Delta)^{3}} \right),$$

and so

(B.1)
$$z(t) = -i\Delta \frac{\partial \alpha}{\partial \omega} (\mu + i\Delta, t) + \alpha(\mu + i\Delta, t),$$

where $\frac{\partial \alpha}{\partial \omega}(\mu + i\Delta, t) = \frac{\partial \alpha}{\partial \omega}(\omega, t)|_{\omega = \mu + i\Delta}$. Taking the derivative with respect to time on both sides and then using (2.10), we get

$$\begin{split} \dot{z}(t) &= -i\Delta \frac{\partial}{\partial \omega} \left(\frac{\partial \alpha}{\partial t}(\omega, t) \right) \bigg|_{\omega = \mu + i\Delta} + \frac{\partial \alpha}{\partial t} (\mu + i\Delta, t) \\ &= -i\Delta \frac{\partial}{\partial \omega} \left(i\alpha(\omega, t)\omega - \frac{i}{2} - \frac{i}{2}\alpha^2(\omega, t) - \frac{c_{ee}}{2}\alpha^2(\omega, t)\overline{z} + \frac{c_{ee}}{2}z \right) \bigg|_{\omega = \mu + i\Delta} \\ &+ i(\mu + i\Delta)\alpha(\mu + i\Delta, t) - \frac{i}{2} - \frac{i}{2}\alpha^2(\mu + i\Delta, t) - \frac{c_{ee}}{2}\alpha^2(\mu + i\Delta, t)\overline{z} + \frac{c_{ee}}{2}z. \end{split}$$

Let $y = y(t) = \alpha(\mu + i\Delta, t)$. Then we have

$$\begin{split} \dot{z} &= -i\Delta \bigg(i(\mu + i\Delta) \frac{\partial \alpha}{\partial \omega} (\mu + i\Delta, t) + iy - iy \frac{\partial \alpha}{\partial \omega} (\mu + i\Delta, t) - c_{ee}y \overline{z} \frac{\partial \alpha}{\partial \omega} (\mu + i\Delta, t) \bigg) \\ &+ (i\mu - \Delta)y - \frac{i}{2} - \frac{i}{2}y^2 - \frac{c_{ee}}{2}y^2 \overline{z} + \frac{c_{ee}}{2}z \\ &= -i\Delta \frac{\partial \alpha}{\partial \omega} (\mu + i\Delta, t) \big(i\mu - \Delta - iy - c_{ee}y \overline{z} \big) + i\mu y - \frac{i}{2} - \frac{i}{2}y^2 - \frac{c_{ee}}{2}y^2 \overline{z} + \frac{c_{ee}}{2}z \\ &= (z - y)(i\mu - \Delta - iy - c_{ee}y \overline{z}) + i\mu y - \frac{i}{2} - \frac{i}{2}y^2 - \frac{c_{ee}}{2}y^2 \overline{z} + \frac{c_{ee}}{2}z, \end{split}$$

where we used (B.1). The equation for \dot{y} uses (2.10) and so, putting them together,

(B.2)
$$\dot{y} = i\mu y - \Delta y - \frac{i}{2}y^2 - \frac{i}{2} - \frac{c_{ee}}{2}y^2 \overline{z} + \frac{c_{ee}}{2}z$$

$$\dot{z} = i\mu z - \Delta z + \Delta y - iyz + \frac{i}{2}y^2 - c_{ee}yz\overline{z} + \frac{c_{ee}}{2}y^2\overline{z} - \frac{i}{2} + \frac{c_{ee}}{2}z.$$

As before, letting $y(t) = r(t)e^{i\theta(t)}$ and $z(t) = s(t)e^{i\phi(t)}$, we arrive at (2.15).

Appendix C. Cusp curve for rescaling analysis. We begin the proof of $c_{cusp}(\mu)$ by eliminating the subscripts as before in (2.19). Since the cusp occurs at a fixed point, $\dot{r} = \dot{\theta} = 0$ and so $\theta = c + 1/r$. Thus, $\dot{\theta} = -\dot{r}/r^2$. Solving for \dot{r} and using (2.19), we have

$$\dot{r} = -r^2 \left(\frac{1}{2} (c + 1/r)^2 - \frac{1}{2} r^2 - bcr + \mu \right) = \frac{1}{2} \left(r^4 + 2bcr^3 - (c^2 + 2\mu)r^2 - 2cr - 1 \right) =: \frac{1}{2} f(r).$$

Now that θ has been eliminated from the system of equations, we can work with f(r) alone. At the cusp bifurcation specifically, we know that f(r) = f'(r) = f''(r) = 0. So we have three equations:

(C.1)
$$r^4 + 2bcr^3 - (c^2 + 2\mu)r^2 - 2cr - 1 = 0$$

(C.2)
$$2r^3 + 3bcr^2 - (c^2 + 2\mu)r - c = 0$$

(C.3)
$$6r^2 + 6bcr - (c^2 + 2\mu) = 0.$$

Our task is to eliminate r and b. Begin by multiplying (C.2) by 2r and subtracting it from (C.1). Also, multiply (C.2) by r and subtract off (C.1). Respectively, we arrive at

(C.4)
$$-3r^4 - 4bcr^3 + (c^2 + 2\mu)r^2 - 1 = 0$$

(C.5)
$$r^4 + bcr^3 + cr + 1 = 0.$$

Next, multiply (C.3) by $2r^2$, and add it to three times (C.4), and multiply (C.3) by r^2 , and subtract it from six times (C.5). This results in our two main equations with b removed:

(C.6)
$$3r^4 + (c^2 + 2\mu)r^2 - 3 = 0$$

(C.7)
$$(c^2 + 2\mu)r^2 + 6cr + 6 = 0$$

Now we solve for r^2 in (C.6), and we set it equal to the square of the solution for r in (C.7). Keeping in mind that r is negative, we find

$$\frac{-(c^2+2\mu)+\sqrt{(c^2+2\mu)^2+36}}{6} = \left(\frac{-3c+\sqrt{3c^2-12\mu}}{c^2+2\mu}\right)^2.$$

Distributing the right-hand side and putting the radicals on one side, one has

$$(c^{2} + 2\mu)^{2} \sqrt{(c^{2} + 2\mu)^{2} + 36} + 36c\sqrt{3c^{2} - 12\mu} = 72(c^{2} - \mu) + (c^{2} + 2\mu)^{3}.$$

Squaring both sides and simplifying yet again by putting the radicals on one side, we see

$$2c\sqrt{(c^2+2\mu)^2+36}\sqrt{3c^2-12\mu}=3c^4+12(3-\mu^2).$$

We square both sides one last time and notice this is a fourth order polynomial in c^2 , and we can use the quartic formula to obtain $c_{cusp}(\mu)$. It is important to note the coefficient of c^6 is zero once you square both sides, which will greatly simplify the curve equation. Lastly, even though we cannot find μ_{cusp} and c_{cusp} in terms of a general b, we list some properties for $(\mu_{cusp}(b), c_{cusp}(b))$:

- 1. $(\mu_{cusp}(1), c_{cusp}(1)) = (-1/2, 1);$
- 2. $(\mu_{cusp}(0), c_{cusp}(0)) = (3^{-3/2}, 4(3^{-3/4})) \approx (0.19245, 1.75477);$
- 3. $\mu_{cusp}(b^*) = 0$ when $b^* = \frac{1}{3}\sqrt{2\sqrt{3} 3} \approx 0.227083$ and $c_{cusp}(b^*) = \sqrt[4]{12(2\sqrt{3} 3)} \approx 1.5362$:
- 4. $\lim_{b\to\infty}(\mu_{cusp}(b), c_{cusp}(b)) = (-\sqrt{3}, 0);$
- 5. $c_{cusp} \sim 1/b$ and $\mu_{cusp} + \sqrt{3} \sim 1/b$ for b large.

REFERENCES

- [1] R. L. STRATONOVICH, Topics in the Theory of Random Noise Vol. 2, Gordon and Breach, New York, 1967.
- [2] C. Kurrer and K. Schulten, *Noise-induced synchronous neuronal oscillations*, Phys. Rev. E, 51 (1995), 6213.
- [3] Y. M. LAI AND M. A. PORTER, Noise-Induced Synchronization, Desynchronization, and clustering in globally coupled nonidentical oscillators, Phys. Rev. E, 88 (2013), 012905.
- [4] M. Scheutzow, Noise can create periodic behavior and stabilize nonlinear diffusions, Stoch. Proc. Appl., 20 (1985), pp. 323–331.
- [5] L. GLASS, P. HUNTER, AND A. MCCULLOCH, EDS., Theory of Heart: Biomechanics, Biophysics, and Nonlinear Dynamics of Cardiac Function, Springer Science & Business Media, New York, 2012.
- [6] J. RINZEL, AND G. B. ERMENTROUT, Analysis of neural excitability and oscillations, Methods in neuronal modeling, 2 (1998), pp. 251–292.
- [7] A. P. LEBEAU, ET AL., Modeling of membrane excitability in gonadotropin-releasing hormone-secreting hypothalamic neurons regulated by Ca2+-mobilizing and adenylyl cyclase-coupled receptors, J. Neurosci, 20 (2000), pp. 9290–9297.
- [8] H. SAKAGUCHI, S. SHINOMOTO, Y. KURAMOTO, Phase transitions and their bifurcation analysis in a large population of active rotators with mean-field coupling, Prog. Theor. Exp. Phys., 79 (1988), pp. 600-607.
- [9] A. Neiman, L. Schimansky-Geier, A. Cornell-Bell, F. Moss, Noise-enhanced phase synchronization in excitable media, Phys. Rev. Lett, 83 (1999), pp. 4896–4899.
- [10] B. LINDNER, J. GARCÍA-OJALVO, A. NEIMAN, L. SCHIMANSKY-GEIER, Effects of noise in excitable systems, Phys. Rep, 392 (2004), pp. 321–424.
- [11] M. Zaks, X. Sailer, L. Schimansky-Geier, and A. Neiman, Noise induced complexity: From subthreshold oscillations to spiking in coupled excitable systems, Chaos, 15 (2005), 026117.
- [12] E. LUÇON AND C. POQUET, Emergence of oscillatory behaviors for excitable systems with noise and mean-field interaction, a slow-fast dynamics approach, Commun. Math. Phys., 373 (2020), pp. 907– 969.
- [13] A. FAISAL, L. SELEN, AND D. WOLPERT, Noise in the nervous system, Nat. Rev. Neurosci., 9 (2008), pp. 292–303.
- [14] J. D. TOUBOUL, C. PIETTE, L. VENANCE, AND G. B. ERMENTROUT, Noise-induced synchronization and antiresonance in interacting excitable systems: Applications to deep brain stimulation in Parkinson's disease, Phys. Rev. X, 10 (2020), 011073.
- [15] A. Neiman, X. Pei, D. Russell, W. Wojtenek, L. Wilkens, F. Moss, H. Braun, M. Huber, and K. Voigt, Synchronization of the noisy electrosensitive cells in the paddlefish, Phys. Rev. Lett, 82 (1999), pp. 660–663.
- [16] L. M. Alonso, G. B. Mindlin, Average dynamics of a driven set of globally coupled excitable units, Chaos, 21 (2011), 023102.

- [17] R. E. LEE DEVILLE, E. VANDEN-EIJNDEN, AND C. B. MURATOV, Two distinct mechanisms of coherence in randomly perturbed dynamical systems, Phys. Rev. E, 72 (2005), 031105.
- [18] J. TOUBOUL, G. HERMANN, AND O. FAUGERAS, Noise-induced behaviors in neural mean field dynamics, SIAM J. Appl. Dyn. Syst., 11 (2012), pp. 49–81.
- [19] K. DIERKES, F. JÜLICHER, AND B. LINDNER, A mean-field approach to elastically coupled hair bundles, Eur. Phys. J. E, 35 (2012), pp. 37–51.
- [20] B. Sonnenschein, M. Zaks, A. Neiman, L. Schimansky-Geier, Excitable elements controlled by noise and network structure, EPJ ST, 222 (2013), pp. 2517–2529.
- [21] E. Ott and T.M. Antonsen, Low dimensional behavior of large systems of globally coupled oscillators, Chaos, 18 (2008), 037113.
- [22] J. G. RESTREPO AND E. Ott, Mean-field theory of assortative networks of phase oscillators, EPL, 107 (2014), 60006.
- [23] K. P. O'KEEFFE AND S. H. STROGATZ, Dynamics of a population of oscillatory and excitable elements, Phys. Rev. E, 93 (2016), 062203.
- [24] L. F. LAFUERZA, P. COLET, R. TORAL, Nonuniversal results induced by diversity distribution in coupled excitable systems, Phys. Rev. Lett., 105 (2010), 084101.
- [25] N. G. Stocks, Suprathreshold stochastic resonance in multilevel threshold systems, Phys. Rev. Lett., 84 (2000), pp. 2310–2313.
- [26] H. SAKAGUCHI, T. OKITA, Cooperative dynamics in coupled systems of fast and slow phase oscillators, Phys. Rev. E, 93 (2016), 022212.
- [27] Y. KAWAMURA, H. NAKAO, Y. KURAMOTO, Collective phase description of globally coupled excitable elements, Phys. Rev. E, 84 (2011), 046211.
- [28] A. K. ALIJANI, M. J.E. RICHARDSON, Rate response to neurons subject to fast or frozen noise: From stochastic and homogeneous to dynamic and heterogeneous populations, Phys. Rev. E, 84 (2011), 011919.
- [29] I. V. TYULKINA, D. S. GOLDOBIN, L. S. KLIMENKO, A. PIKOVSKY, Dynamics of noisy oscillator populations beyond the Ott-Antonsen ansatz, Phys. Rev. Lett., 120 (2018), 264101.
- [30] J. BUCETA, J. M. PARRONDO, C. VAN DEN BROECK, AND F. J. DE LA RUBIA, Negative resistance and anomalous hysteresis in a collective molecular motor, Phys. Rev. E, 61 (2000), pp. 6287–6293.
- [31] J. A. Bonachela, C. D. Nadell, J. B. Xavier, et al., *Universality in bacterial colonies*, J. Stat. Phys., 144 (2011), pp. 303–315.
- [32] M. Beiran, A. Kruscha, J. Benda, and B. Lindner, Coding of time-dependent stimuli and homogeneous and heterogeneous neural populations, J. Comp. Neurosci., 44 (2018), pp. 189–202.
- [33] E. MONTBRIÓ, D. PAZÓ, AND A. ROXIN, Macroscopic description for networks of spiking neurons, Phys. Rev. X, 5 (2015), 021028.
- [34] Y. A. KUZNETSOV, Elements of Applied Bifurcation Theory, Springer-Verlag, Berlin, Heidelberg, 1998.
- [35] J. Guckenheimer, and I. S. Labouriau, Bifurcation of the Hodgkin and Huxley equations: A new twist, Bull. Math. Biol., 55 (1993), pp. 937-952.
- [36] N. KOPELL, AND G. B. ERMENTROUT, Symmetry and phaselocking in chains of weakly coupled oscillators, Commun. Pure Appl. Math., 39 (1986), pp. 623-660.
- [37] G. B. Ermentrout, A heuristic description of spiral wave instability in discrete media, Physica D: Nonlinear Phenomena, 82 (1995), pp. 154–164.
- [38] Y. Kuramoto, and D. Battogtokh, Coexistence of coherence and incoherence in nonlocally coupled phase oscillators, preprint, arXiv:cond-mat/0210694.
- [39] D. Orr and G. B. Ermentrout, Synchronization of oscillators via active media, Phys. Rev. E, 99 (2019), 052218.
- [40] S. Coombes and A. Byrne, Next generation neural mass models, Nonlinear Dynamics in Computational Neuroscience, Springer, Cham, 2019, pp. 1–16.
- [41] C. Bick, M. Goodfellow, C. R. Laing, and E. A. Martens, Understanding the dynamics of biological and neural oscillator networks through exact mean-field reductions: A review, J. Math. Neurosc., 10 (2020), pp. 1–43.